

Supplemental Information

Structural and Chemical Properties of NiO_x Thin Films: The Role of Oxygen Vacancies in NiOOH Formation in H₂O Atmosphere

Raoul Blume, Wolfram Calvet, Aliakbar Ghafari, Thomas Mayer, Axel-Knop-Gericke, Robert Schlögl

*,^a Max-Planck-Institut für Chemische Energiekonversion, Postfach 101365, 45413 Mülheim an der Ruhr, Germany.

E-mail: raoul@fhi-berlin.mpg.de

^b Fachbereich 1, Umweltbundesamt, Wörlitzer Platz 1, 06844 Dessau-Roßlar, Germany.

^c FG Oberflächenforschung, TU Darmstadt, Otto-Berndt-Str. 3, 64287 Darmstadt, Germany.

^d Abt. Anorganische Chemie, Fritz-Haber-Institut der MPG, Faradayweg 4-6, 14195 Berlin, Germany.

Fit Model and Quantification	2
Sample characterization	4
Oxygen vacancy formation on NiO _x during heating up 650°C in O ₂ atmosphere	6
Heating – cooling cycles in O ₂ atmosphere	7
Structural changes of NiO in contact with O ₂ at elevated temperatures	8
NiO in contact with water vapour at elevated temperatures	10
XAS comparison of oxygen vacancies in O ₂ and H ₂ O atmosphere	12

Fit Model and Quantification

Ni2p _{3/2}	metal	NiO 1	NiO 2	NiO 3	NiO 4	NiO 5		
BE (eV)	852,5	853,75	855,5	861	863,9	866.1 - 866.6		
α	0,13							
FWHM (eV)	1,2	1,2	2,8	4 (O ₂) / 3.5 (H ₂ O)		2,3	3,3	
O1s	NiO _{1-x}	NiO	Ni _{1-x} -OH	NiOOH	Ni ₂ O ₃ /Ni(OH) ₂	NiOOH	NiO-H ₂ O _{ad}	H ₂ O-H ₂ O
BE (eV) @								
1000 eV	528,9	529,4	529,95	530,6	531,2	531,8	532,7	533,6
880 eV		529,4				531,9		
680 eV		529,4				532		
FWHM (eV)	1	1	1,2	1,2	1,2	1,2	1,2	1,2

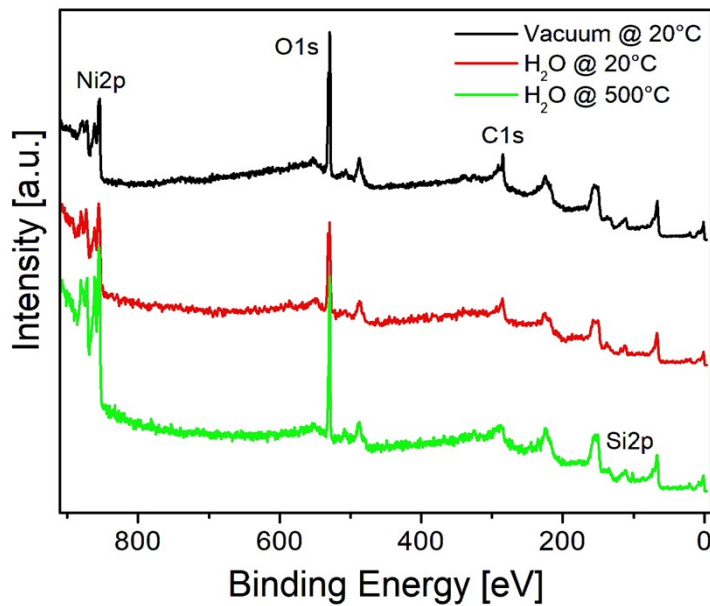
SI-Table 1: Fit components and parameter used in the fit model.

Binding energies (BE) of the Ni2p, O1s and VB spectra were calibrated to the metal Fermi edge still visible during oxide growth. Where no metal was present oxide spectra were adjusted to the oxide positions observed during oxide growth. As the first step of XPS analysis and fitting procedures a Shirley-type background correction was applied.¹ Spectra were fitted following the Levenberg-Marquardt algorithm to minimize the standard deviation expressed by the chi-square value χ^2 . The peak shapes were modelled with Doniach-Sunjic functions convoluted with Gaussian profiles, which allows for the introduction of an asymmetry factor α where required.² An overview of the Ni2p and O1s fits and the applied parameters is given in SI-Table 1. The evaluation of the Ni2p core levels is particularly difficult because of the nature of the photoemission process in nickel oxide and its water related derivatives. Here, various contributions of Ni3d-O2p related transitions result in a spectral signature with a distinct satellite structure. The Ni2p region fits with their satellite structure were performed according to Biesinger et al.^{3,4} FWHM are applied according to the performance of the beamline and the spectrometer. The O1s fits are based on the binding energies reported in references 5,6,7. The accuracy of the binding energy position is $\approx \pm 0.05$ eV. Additional peaks, namely the two components at 528.9 eV and 530 eV are fitted on the basis of the peak shapes, widths and positions expected of the NiO and neighboring NiOOH peaks. Note, that the peak at 531.2 eV can be assigned to Ni-deficient NiO or Ni³⁺ as well as to Ni(OH)₂. For the sake of simplicity, we fitted only one peak and allowed for small shifts in the spectra to account for the respective major contribution.

By assuming a homogeneous mixture of Ni and O, quantification of the sample composition was performed according to $C_x = n_x / \sum n_{x,y}$, with $n_x = I(x) / S_x$ and $S_x = \sigma \lambda_{total}$ (λ_{total} : electron escape depth; σ : cross-section). S_{oxygen} was determined by fitting the spectrum of a freshly prepared NiO and assuming the intensity of the full Ni2p and the O1s NiO component as 1:1 NiO. S_{Ni} was determined using σ and λ_{total} calculated according to Yeh et al. and Seah, respectively.^{8,9} It needs to be mentioned, that, with the assumption of a homogeneous mixed composition, XPS quantification is rather rough and could potentially lead to a systematic error yielding an offset of the Ni and O fractions in NiO. Thus, it should be seen as a guideline to follow changes in the composition of the samples presented here. Quantitative analysis of depth profiles (not shown here) indicates that apart from such offset the

compositional changes observed for different depths exhibit the same trends. This allows to estimate an error for these changes (excluding the offset) in the range of only $\pm 2 - 3 \%$. (See also SI-Figures 4 and 7). Thus, the quantification method applied effectively reflects the evolution of the sample composition in dependence of temperature.

Sample characterization

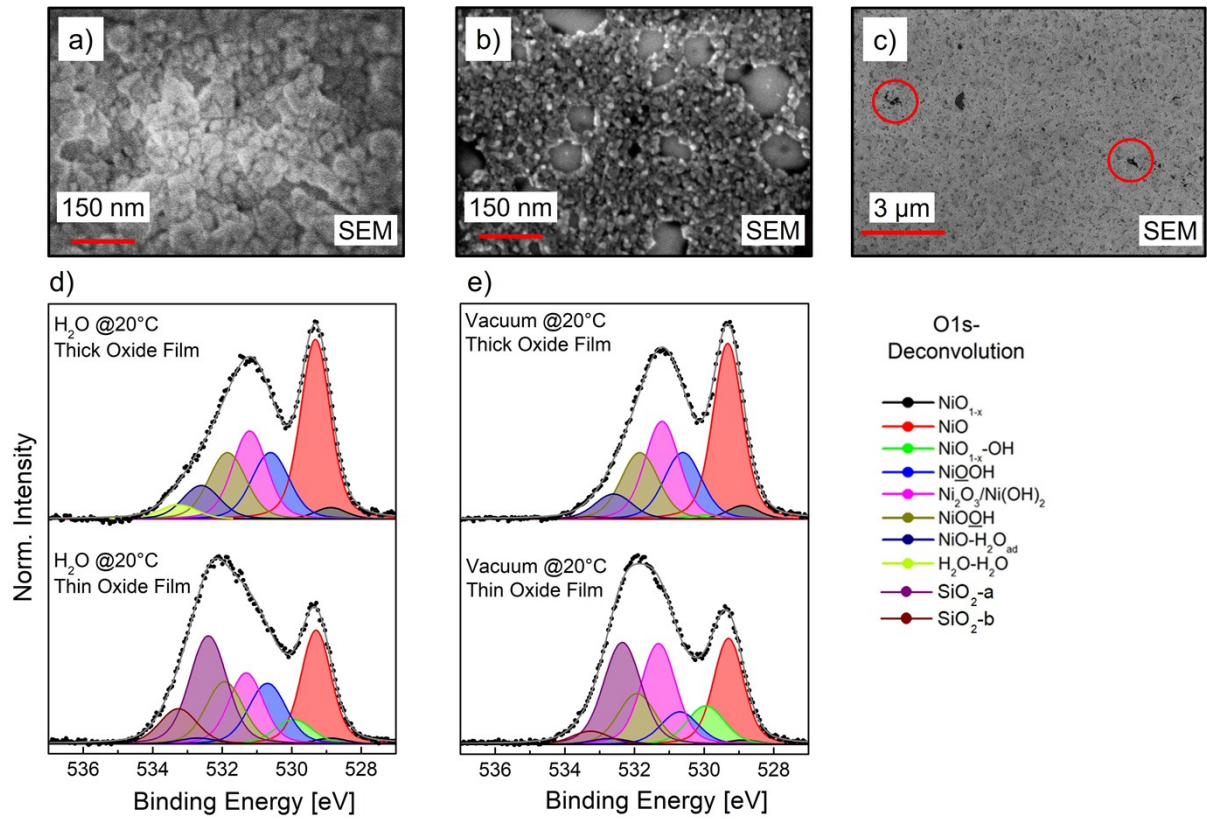


SI-Figure 1: Survey spectra recorded before and during heating in 0.5 mbar H₂O at different temperatures.

The topmost spectrum in SI-Figure 1 depicts typical surveys of NiO_x thin films before exposure to O₂ or H₂O. Some residual carbon is present which vanishes completely after heating above $\approx 250^\circ\text{C}$ in O₂ or H₂O and only re-emerges at lower quantities after cooling and evacuation at the end of the experiment.

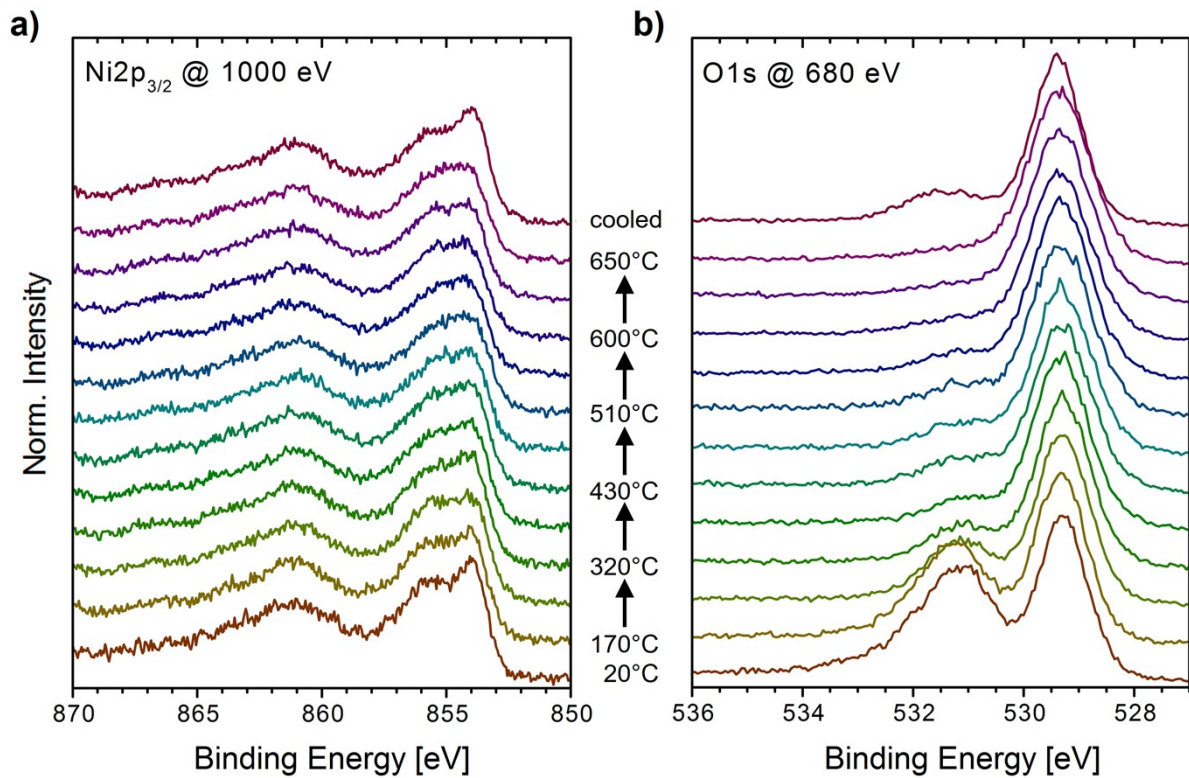
Si contaminations and their potential contribution to the O1s spectra were checked by survey spectra as well as Si2p spectra (not shown). As can be seen in SI-Figure 1, bottom panel, some Si appears on the sample surface when heated to 500°C. SI-Figure 2 a) shows that a thick NiO_x film, representative for II used in the main paper, is forming a particle-like surface but is not de-wetting. However, there are pinholes present which are the reason for the presence of small amounts of SiO₂. On the other hand, a thinner 50 nm NiO_x film heated to 500°C exhibits a partial de-wetting of the film (SI-Figure 2 b). A comparison of the O1s spectra of both films show that SiO₂ contributions to the O1s region of the thicker film, which are located on the high BE side of the spectra, can be neglected. This is further corroborated by the expected behavior of H₂O-adsorption-related peaks to the presence of large amounts of water. In addition, apart from the two high BE peaks, even for a thinner 50 nm film all spectral components related to oxygen vacancies and all Ni-OH bonds evolve exactly like those of a thick film. Hence, the immense spectral and structural changes observed in our experiments are not caused by SiO₂ contaminants.

Preparation: film SI-Figure 2 a) and c) total oxygen exposure 272 min O₂; H₂O exposure 264 min; film SI-Figure 2 b): total oxygen exposure 176 min O₂; H₂O exposure 341 min.



SI-Figure 2: a) SEM micrographs of oxidized 200 nm Ni-film and b) an oxidized thinner 50 nm NiO film, both after three heating cooling cycles in 0.5 mbar H₂O. d) and e) O1s spectra corresponding to a) and b), respectively, recorded in 0.5 mbar H₂O and after evacuation at RT. c) Large-scale SEM micrograph of the 200 nm NiO film of a) with pinholes in the film (red circles).

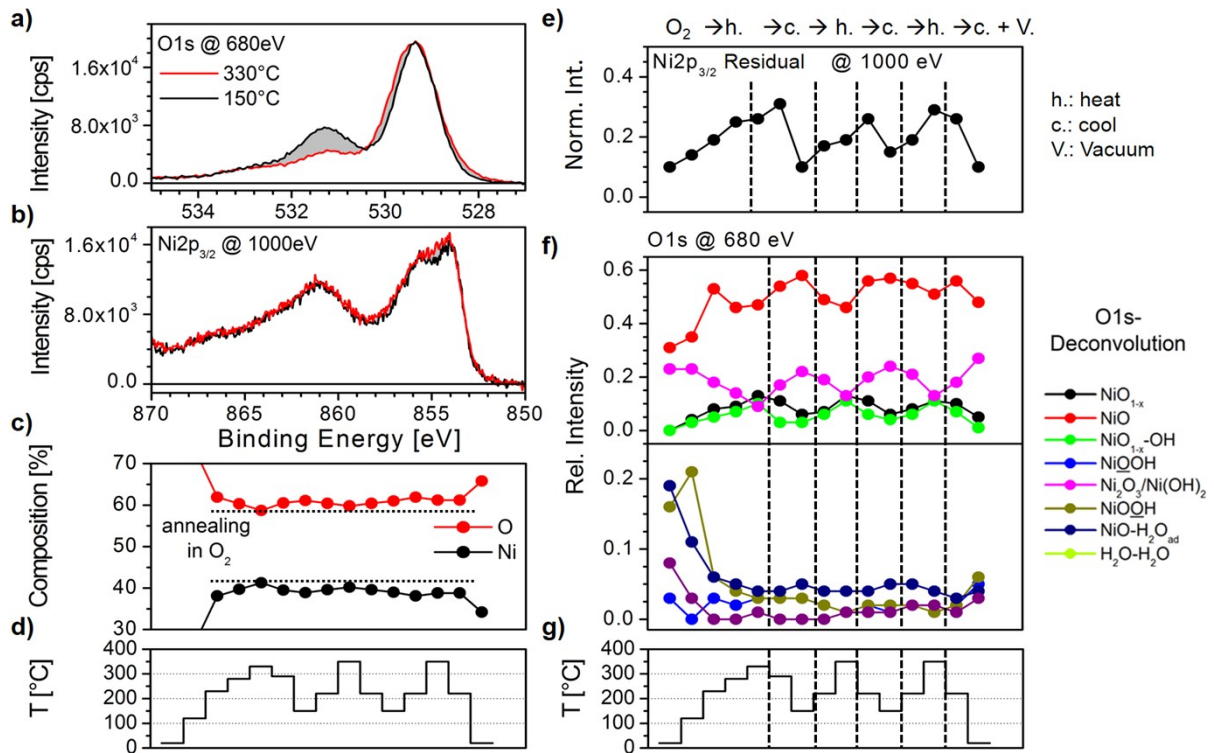
Oxygen vacancy formation on NiO_x during heating up 650°C in O₂ atmosphere



SI-Figure 3: a) Ni 2p_{3/2} spectra during heating to 650°C in 0.5 mbar O₂ atmosphere and subsequent cooling to RT. b) O 1s spectra corresponding to a). The same color indicates the same temperature in each region.

SI-Figure 3 shows the complete Ni 2p_{3/2} and O 1s data sets recorded during heating of a NiO_x film to 650°C and subsequent cooling to RT in 0.5 mbar O₂ atmosphere corresponding to Figures 1 and 2 of the main text.

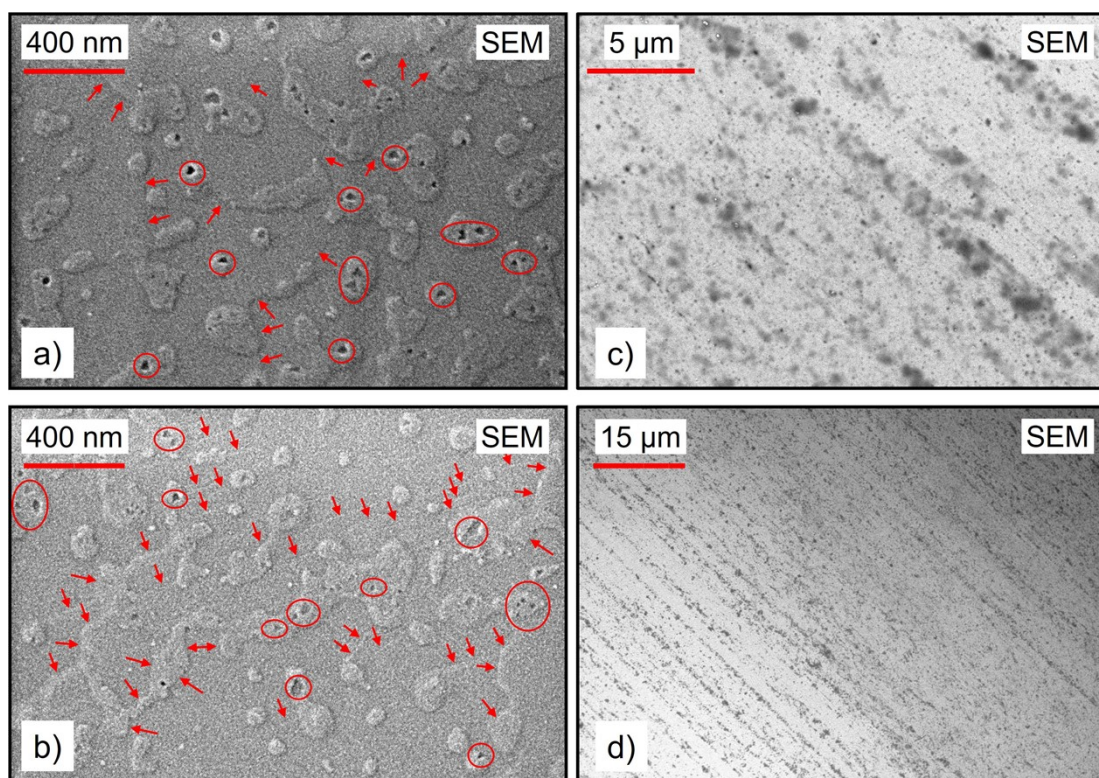
Heating – cooling cycles in O₂ atmosphere



SI-Figure 4: XP spectra recorded during heating in 0.5 mbar O₂: a) O1s spectra recorded at the first temperature maximum and minimum at 330°C and 150°C, respectively. b) Ni2p_{3/2} spectra corresponding to a). The intensities are normalized. c) Sample composition calculated from the XPS for the complete heating-cooling experiment. e) Evolution of the Ni2p_{3/2} residuum derived from subtracting a fit of the pure NiO from the measured spectrum (grey areas in b) with temperature. f) Evolution of the relative intensities of oxygen species as derived from the fits of the O1s spectra with temperature. The fits were performed according to the peak components listed in SI-Table 1. Note that the photon energies for the O1s and Ni2p_{3/2} spectra represent the same information depth. d) and g) Heating profiles.

SI-Figure 4 illustrates the spectral evolution induced by the heating – cooling cycles up to 350°C in oxygen atmosphere. While the initial broadening of the main NiO O1s peak and the flattening of the Ni2p_{3/2} main peak (SI-Figure 2 a) and e), respectively) are very similar to what is observed during heating-cooling cycles in H₂O there is no notable intensity gain in the high BE region above the main NiO peak in the O1s region (SI-Figures 4 a) and f) compared to the same treatment in H₂O. This is reflected in the marginal oxygen uptake visible in SI-Figure 2 c). Similarly, the relative intensities of the OH-related bonds do not show any significant increase during the treatment which, not surprisingly, would be considerable after the treatment in H₂O (see main text).

Structural changes of NiO in contact with O₂ at elevated temperatures



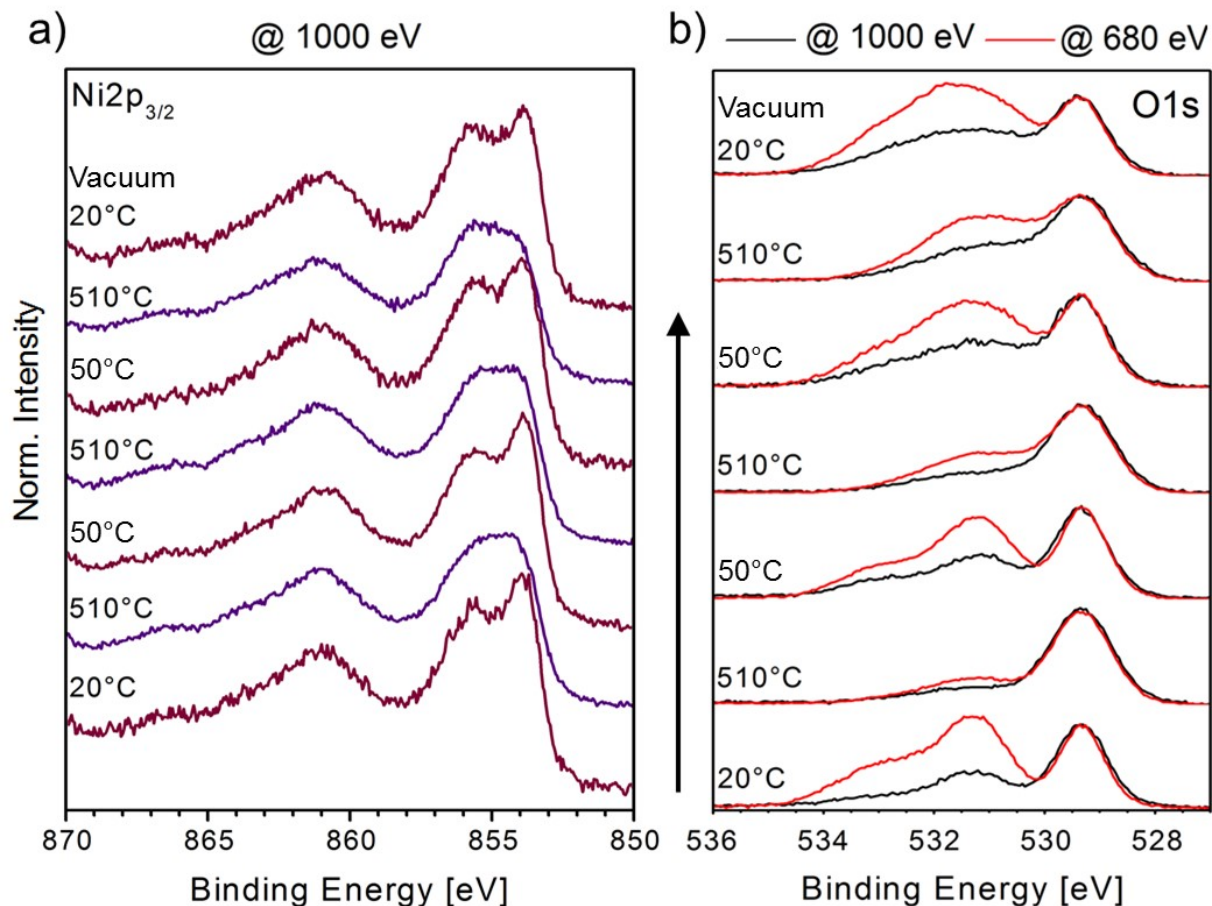
SI-Figure 5: Ex-situ SEM micrographs of a) the as-prepared NiO_x sample, b) after two heating-cooling cycles and c) & d) after three heating-cooling cycles to 350°C in O₂ atmosphere, respectively. Step edges in a) and b) are indicated by red arrows while red circles mark the presence of triangular shaped holes. In Figures c) and d) step edges are visible by carbon accumulation due to exposure to air before SEM measurements.

By applying multiple heating-cooling cycles to 350°C, oxygen vacancy formation is reversible to a certain extent (SI-Figure 4). We observed that, while the Ni2p_{3/2} residuum fully vanishes, both, the NiO_{1-x} and the NiO_{1-x}-OH peak retain some intensity even after cooling which suggests a more defective surface than the as-prepared NiO_x film.¹⁹ Indeed, repeated heating-cooling cycles in oxygen affect the morphology of the NiO_x sample as well. SI-Figure 5 depicts SEM micrographs of a NiO_x sample before (a), after two (b) and after three (c) and d) heating-cooling cycles to 350°C in 0.5 mbar of O₂. The as-prepared NiO_x film appears mainly flat with only a small number of visible step edges or terraces. Moreover, rather inhomogeneous, protruding areas are present which suggests the presence of more than one surface orientation. On closer inspection, the boundaries of the protruding areas feature some hexagonal and triangular shapes as well as mainly triangular cavities in the center of those areas. When characterized with XRD, a Ni film oxidized under the described conditions usually consists mainly of (200) oriented areas with some contributions of (111) and (110) orientations.^{10,11,12} Hence, the flat sample areas are most likely related to NiO(100), also because this represents the most stable NiO orientation.^{13,14,15} On the other hand, the hexagonal and triangular shapes of the protruding areas as well as the triangular holes within may indicate the presence of NiO(111). The coexistence of NiO(111) on NiO(100) on surfaces has been reported before.^{16,17} The morphology changes after annealing in O₂. The flat sample areas become visibly terraced even detectable with SEM, indicated by red arrows in SI-Figure 5 b). The number of protruding areas seems to decrease while their remaining areas coagulate

predominantly at step edges thus forming a cross-linked structure with elongated extensions that are up to several micrometers long and ~ 50 nm wide. Their boundaries still feature hexagonal and triangular shapes (red circles). This behavior fits to the assignment of these features to NiO(111) which is expected to be unstable above $220\text{ }^{\circ}\text{C}$ ¹⁴ and, thus, would explain their area loss and coagulation. After three heating-cooling cycles the increase of step-edge formation is even more apparent by the carbon accumulation due to exposure to air before SEM measurements.

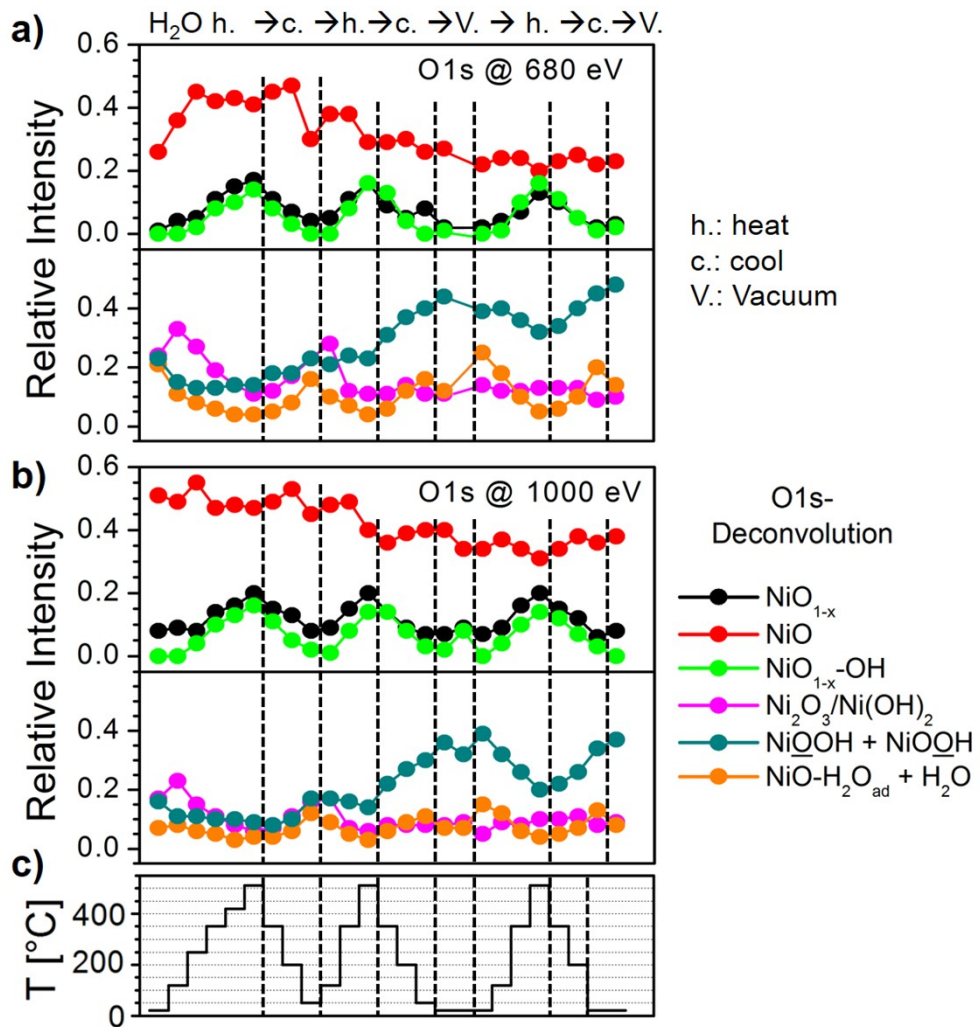
Preparation: film SI-Figure 5 a) and b): total oxygen exposure 155 min O_2 ; film SI-Figure 5 c) and d): total oxygen exposure 280 min O_2

NiO in contact with water vapour at elevated temperatures



SI-Figure 6: XP spectra recorded during heating-cooling cycles in 0.5 mbar H₂O: a) Ni_{2p}_{3/2} at $h\nu = 1000$ eV, b) O1s depth profiles at selected temperatures in H₂O atmosphere ($h\nu = 1000$ eV and 680 eV). The intensities are normalized to the peaks located at 529.5 eV. Note that the Ni_{2p}_{3/2} at 1000 eV and O1s spectra at 680 eV share the same information depth.

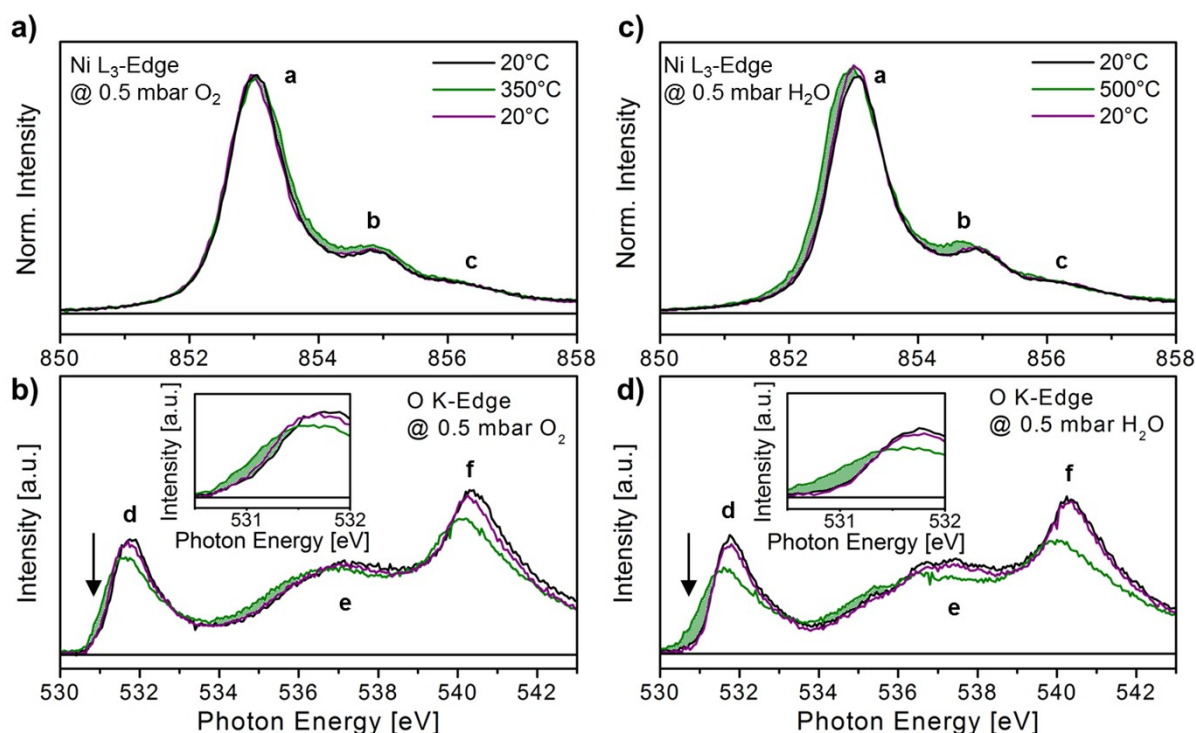
SI-Figure 6 corresponds to Figures 3 and 4 of the main text. SI-Figure 6 a) shows the Ni_{2p}_{3/2} spectra at each T_{\min} and T_{\max} recorded during three heating-cooling cycles in 0.5 mbar H₂O atmosphere and subsequent evacuation. SI-Figure 6 b) depicts the corresponding depth resolved O1s spectra.



SI-Figure 7: Relative intensities of the peaks fitted to the O1s spectra recorded during three heating-cooling cycles in 0.5 mbar H₂O a) $h\nu = 680$ eV and b) $h\nu = 1000$ eV. c) Heating profile.

SI-Figure 7 shows the evolution of the relative intensities obtained from the full sets of O1s fits of a depths profiling at 680 and 1000 eV, respectively, during three heating-cooling cycles in 0.5 mbar H₂O atmosphere.

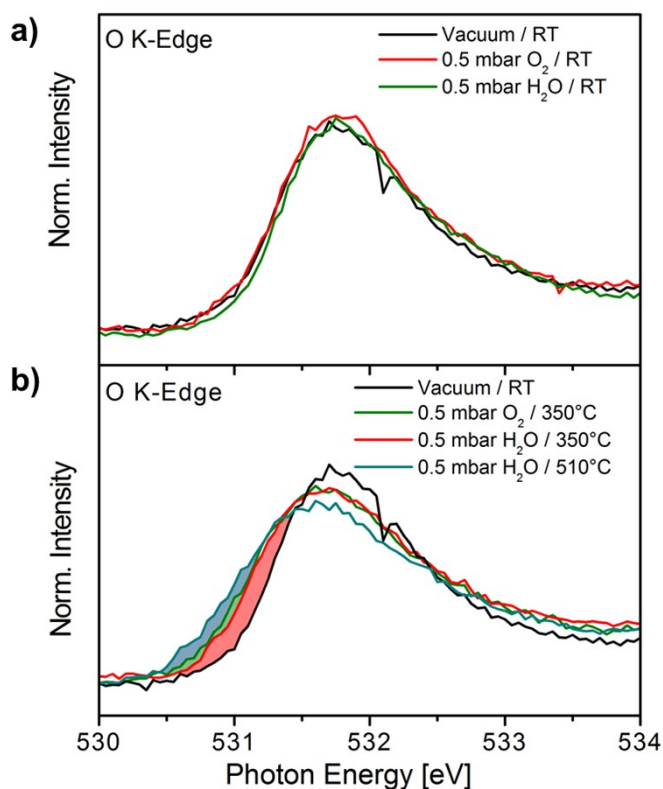
XAS comparison of oxygen vacancies in O₂ and H₂O atmosphere



SI-Figure 8: a) and b) XA spectra of the Ni L₃- and O K-edge of the NiO_x sample at RT, at the third T_{max} and after final cooling in 0.5 mbar O₂ partial pressure, respectively. c) and d) XA spectra of the Ni L₃- and O K-edge, respectively, of the same sample at RT, at the first T_{max} and after the first cooling in 0.5 mbar H₂O partial pressure, corresponding to Figure 5. The features a - f are discussed in the main text.

SI-Figure 8 compares the Ni L₃-edge and O K-edge spectra recorded in 0.5 mbar O₂ and H₂O, respectively. While, in both gases, the spectra recorded at RT are almost identical, at T_{max} the spectra evolve slightly different. It appears that the shift of peaks a and b observed in the Ni L₃-edge as well as the broadening of peak d observed in the O K-edge spectra are more pronounced for the higher temperature applied in H₂O atmosphere.

SI-Figure 9 compares the low energy side of XAS spectra recorded in vacuum (at 20°C only) and 0.5 mbar H₂O atmosphere at 20°C, 350 and 510°C, respectively, to the spectra recorded at 20 and 350°C in 0.5 mbar O₂ atmosphere. The original spectra measured in O₂ atmosphere exhibit a distinct intensity loss at a photon energy of ≈ 531 eV stemming from π* absorption resonance in the O₂ gas phase. By applying a reconstruction procedure, developed by Hävecker et al. and described in detail in references 18 and 19 this feature can be removed yielding the O₂-related spectra displayed in SI-Figure 6 a) and b). All spectra taken at around RT agree well with each other (SI-Figure 5 and 6 a). Similarly, after heating to 350°C as shown in SI-Figure 6 b), both, the O₂ - as well as the H₂O - related spectrum, exhibit the same broadening with respect to the 20°C - vacuum spectrum. The spectrum recorded at 510°C in H₂O shows an even more pronounced broadening as expected from the formation of oxygen vacancies as described in the main text.



SI-Figure 9: a) Reconstructed O K-edge spectrum recorded in 0.5 mbar O₂ atmosphere at 20°C compared to its vacuum and 0.5 mbar H₂O counterparts. b) Reconstructed O K-edge spectrum recorded in 0.5 mbar O₂ atmosphere at 350°C compared to its 0.5 mbar H₂O-350°C counterpart and the spectrum recorded at 20°C in vacuum.

1 D.A. Shirley, *Phys. Rev. B*, 1972, **5**, 4709-4714.

2 S. Doniach, M. Sunjic, *J. Phys. C: Solid State Phys.*, 1970, **3**, 285-291.

3 M.C. Biesinger, B.P. Payne, A.P. Grosvenor, L.W.M. Lau, A.R. Gerson, R.St.C. Smart, *Appl. Surf. Sci.*, 2011, **257**, 2717-2730.

4 A.P. Grosvenor, M.C. Biesinger, M.C., R.St.C. Smart, N.S. McIntyre, *Surf. Sci.*, 2006, **600**, 1771-1779.

5 M. Fingerle, S. Tengeler, W. Calvet, T. Mayer, W. Jaegermann, *J. Electrochem. Soc.*, 2018, **165**(4), H3148-H3153.

6 M. Fingerle, S. Tengeler, W. Calvet, W. Jaegermann, T. Mayer, *J. Electrochem. Soc.*, 2020, **167**, 136514 (1-10).

7 F. Ullrich, S. Hillebrandt, S. Hietzschold, V. Rohnacher, T. Marszalek, W. Kowalsky, R. Lovrincic, S. Beck, E. Mankel, A. Pucci, *ACS Appl. Energy Mater.*, 2018, **1**, 3113-3122.

8 J.J. Yeh, I. Lindau, *Atomic Data and Nuclear Data Tables*, 1985, **32**, 1-155.

9 M.P. Seah, *Surface and Interface Analysis*, 1986, **9**, 85-98.

10 V. Patil, S. Pawar, M. Chougule, P. Godse, R. Ratnakar, S. Sen, P. Joshi, *J. Surf. Eng. Mater. Adv. Technol.*, 2011, **1**, 35-41.

11 M.S. Jamal, S.A. Shahahmadi, P. Chelvanathan, H.F. Alharbi, M. R. Karim, M.A. Dar, M. Luqman, N.H. Alharthi, Y.S. Al-Harhi, M. Aminuzzaman, N. Asim, K. Sopian, S.K. Tiong, N. Amin, Md. Akhtaruzzaman, *Results Phys.*, 2019, **14**, 102360.

12 Z. Luo, L. Liu, X. Yang, X. Luo, P. Bi, Z. Fu, A. Pang, W. Li, Y. Yi, *ACS Appl. Mater. Interfaces*, 2020, **12**, 39098-39107.

13 M. Sterrer, H.-J. Freund, in *Surface and Interface Science*, Vol. 3 (Ed. K. Wandelt), Wiley-VCH, Weinheim,

Germany 2013, 229-278.

14 M.A. Langell, M.H. Nassir, *J. Phys. Chem.*, 1995, **99**, 4162-4169.

15 M.A. Munoz-Marquez, R.E. Tanner, D.P. Woodruff, *Surf. Sci.*, 2004, **565**, 1-13.

16 N. Kitakatsu, V. Maurice, C. Hinnen, P. Marcus, *Surf. Sci.*, 1998, **407**, 36-58

17 L. Liu, S. Wang, S. Liu, Q. Guo, J. Guo, *Surf. Sci.*, 2018, **667**, 8-12.

18 M. Hävecker, M. Cavalleri, R. Herbert, R. Follath, A. Knop-Gericke, C. Hess, K. Hermann, R. Schlögl, *Phys. Status Solidi B*, 2009, **246**, 1459-1469.

19 R. Blume, W. Calvet, A. Ghafari, T. Mayer, A. Knop-Gericke, R. Schlögl, *Chem. Phys. Chem.* 2023, submitted.